

# Enhanced Cyan Emission and Optical Tuning of $\text{Ca}_3\text{Ga}_4\text{O}_9:\text{Bi}^{3+}$ for High-Quality Full-Spectrum White Light-Emitting Diodes

Dongjie Liu, Xiaohan Yun, Guogang Li,\* Peipei Dang, Maxim S. Molokeev, Hongzhou Lian, Mengmeng Shang, and Jun Lin\*

Highly efficient cyan-emitting phosphor materials are indispensable for closing the cyan gap in spectra of the traditional phosphor-converted white light-emitting diodes (WLEDs) to achieve high-quality full-spectrum white lighting. In this work, bright cyan-emitting  $\text{Ca}_3\text{Ga}_4\text{O}_9$  (CGO): $0.02\text{Bi}^{3+}, 0.07\text{Zn}^{2+}$  phosphor is developed to bridge the cyan gap. Such a  $\text{Bi}^{3+}, \text{Zn}^{2+}$  codoping enhances the cyan emission of CGO: $0.02\text{Bi}^{3+}$  by 4.1 times due to the influence of morphology and size of phosphor particles, charge compensation and lattice distortion. Interestingly, codoping  $\text{La}^{3+}$  ions into the current system can achieve a photoluminescence tuning of CGO: $0.02\text{Bi}^{3+}$  from cyan to yellowish-green by crystallographic site engineering. Besides,  $\text{Bi}^{3+}-\text{Eu}^{3+}$  energy transfer is successfully realized in CGO: $0.02\text{Bi}^{3+}, 0.07\text{Zn}^{2+}, n\text{Eu}^{3+}$  phosphors and the emission color tuning from cyan to orange is observed. The investigation of thermal quenching behaviors reveals that the incorporation of  $\text{Zn}^{2+}$  and  $\text{La}^{3+}$  improves the thermal stability of CGO: $0.02\text{Bi}^{3+}$ . Finally, CGO: $0.02\text{Bi}^{3+}, 0.07\text{Zn}^{2+}, 0.10\text{Eu}^{3+}$  phosphor is employed to obtain a single-phased warm WLED device. A full-spectrum WLED device with remarkable color rendering index (Ra) of 97.4 and high luminous efficiency of  $69.72 \text{ lm W}^{-1}$  is generated by utilizing CGO: $0.02\text{Bi}^{3+}, 0.07\text{Zn}^{2+}$  phosphor. This result suggests the important effect of CGO: $0.02\text{Bi}^{3+}, 0.07\text{Zn}^{2+}$  phosphor on closing the cyan gap, providing new insights of cyan-emitting phosphors applied in full-spectrum white lighting.


## 1. Introduction

Nowadays, phosphor-converted white light-emitting diodes (pc-WLEDs) have attracted widespread attention and been widely developed due to their prominent advantages over the traditional light sources, including energy saving, longer operating lifetimes, high luminous efficacy and environmental friendliness.<sup>[1]</sup> Generally, WLEDs are manufactured by coating YAG:Ce yellow phosphors on the blue LED chips.<sup>[2]</sup> However, this combination gives a low color rendering index (Ra < 75) and a high correlated color temperature (CCT > 4500 K) because of the insufficient red component in emission.<sup>[3]</sup> Moreover, the strong blue light generated by the blue LED chip is harmful to human health.<sup>[4]</sup> One improved approach is to fabricate a WLED device using a near-ultraviolet (n-UV, 360–420 nm) LED chip coated with a mixture of tricolor phosphors, such as blue-emitting  $\text{BaAl}_2\text{O}_9:\text{Eu}^{2+}$  phosphor, green-emitting  $\beta\text{-SiAlON}:\text{Eu}^{2+}$  phosphor, and red-emitting  $\text{CaAlSiN}_3:\text{Eu}^{2+}$

Dr. D. J. Liu, Dr. P. P. Dang, Dr. H. Z. Lian, Prof. J. Lin  
State Key Laboratory of Rare Earth Resource Utilization  
Changchun Institute of Applied Chemistry  
Chinese Academy of Sciences  
Changchun 130022, P. R. China  
E-mail: jlin@ciac.ac.cn

Dr. D. J. Liu, Dr. P. P. Dang, Prof. J. Lin  
School of Applied Chemistry and Engineering  
University of Science and Technology of China  
Hefei 230026, China

Dr. X. H. Yun, Prof. G. G. Li  
Engineering Research Center of Nano-Geomaterials of  
Ministry of Education  
Faculty of Materials Science and Chemistry  
China University of Geosciences  
Wuhan 430074, P. R. China  
E-mail: ggli@cug.edu.cn

 The ORCID identification number(s) for the author(s) of this article can be found under <https://doi.org/10.1002/adom.202001037>.

DOI: 10.1002/adom.202001037

Prof. M. S. Molokeev  
Laboratory of Crystal Physics  
Kirensky Institute of Physics  
Federal Research Center KSC SB RAS  
Krasnoyarsk 660036, Russia

Prof. M. S. Molokeev  
Department of Engineering Physics and Radioelectronics  
Siberian Federal University  
Krasnoyarsk 660041, Russia

Prof. M. S. Molokeev  
Department of Physics  
Far Eastern State Transport University  
Khabarovsk 680021, Russia

Prof. M. M. Shang  
School of Material Science and Engineering  
Shandong University  
Jinan 266071, P. R. China

Prof. J. Lin  
School of Applied Physics and Materials  
Wuyi University  
Jiangmen, Guangdong 529020, P. R. China

phosphor.<sup>[5]</sup> Although this kind of WLED can produce warm white light and reduce the blue light hazard, the limitation still exists. That is an obvious spectrum gap appearing in the cyan region (480–520 nm) of the visible spectrum, making it challenging to realize the full-spectrum lighting that resembles sunlight.<sup>[6]</sup> To address this issue, an efficient cyan-emitting phosphor is desired to close the cyan gap, which is indispensable to achieve high-quality lighting with ultra-high color rendering.

Accordingly, a competitive cyan-emitting phosphor is suggested to possess a broad emission band covering the region of 480–520 nm with a peak at  $\approx 490$  nm, high photoluminescence quantum efficiency and excellent thermal stability. Cyan emission is common in  $\text{Eu}^{2+}$  and  $\text{Ce}^{3+}$  activated phosphors. For example,  $\text{Sr}[\text{Be}_6\text{ON}_4]_2\text{Eu}^{2+}$ ,<sup>[7]</sup>  $\text{Na}_{0.5}\text{K}_{0.5}\text{Li}_3\text{SiO}_4\text{:Eu}^{2+}$ ,<sup>[1c]</sup>  $\text{RbBaScSi}_3\text{O}_9\text{:Eu}^{2+}$ ,<sup>[8]</sup> and  $\text{Ca}_2\text{LuScZrAl}_2\text{GeO}_{12}\text{:Ce}^{3+}$ <sup>[9]</sup> have been recently reported. However, the emission spectra of these  $\text{Eu}^{2+}$  doped phosphors are not broad enough to well close the cyan gap. Besides, a visible light reabsorption is usually unavoidable in  $\text{Eu}^{2+}$  and  $\text{Ce}^{3+}$  doped phosphors as they usually exhibit strong absorption bands in the blue-green region, which overlap with the emission spectra.<sup>[10]</sup> As another activator species,  $\text{Bi}^{3+}$  stands out with broad emission band and nearly no reabsorption problem encountered by rare earth ions because it has characteristic excitation in n-UV rather than in the visible region, thereby avoiding the visible light reabsorption.<sup>[11]</sup> There have been several  $\text{Bi}^{3+}$  doped cyan-emitting phosphors such as  $\text{LiGd}_5\text{P}_2\text{O}_{13}\text{:Bi}^{3+}$ ,<sup>[12]</sup>  $\text{SrBaLaGaO}_5\text{:Bi}^{3+}$ ,<sup>[13]</sup> and  $\text{Ba}_{1.5}\text{Sr}_{1.5}\text{Sc}_4\text{O}_9\text{:Bi}^{3+}$ .<sup>[14]</sup> But the excitation energy of  $\text{LiGd}_5\text{P}_2\text{O}_{13}\text{:Bi}^{3+}$  ( $\lambda_{\text{ex}} = 290$  nm) is too high to match well with the n-UV chips typically generating light beyond 360 nm. In addition,  $\text{SrBaLaGaO}_5\text{:Bi}^{3+}$  and  $\text{Ba}_{1.5}\text{Sr}_{1.5}\text{Sc}_4\text{O}_9\text{:Bi}^{3+}$  phosphors have low photoluminescence quantum efficiency (<30%) and poor thermal stability (emission intensity at 423 K is lower than 20% of the room-temperature intensity). Given that the available  $\text{Bi}^{3+}$  activated cyan-emitting phosphors are extremely limited, it is still urgent to exploit an outstanding cyan-emitting phosphor activated by  $\text{Bi}^{3+}$  ions with broad emission band, high luminous efficiency and good thermal stability.

In addition, single-phased white-emitting phosphors have been greatly studied and developed. One of the most commonly adopted strategies for single-phased white emission is to design energy transfer between activators in an appropriate host.<sup>[15]</sup>  $\text{Bi}^{3+}$  is not only an activator but also a sensitizer, which can transfer energy to  $\text{Eu}^{3+}$  in lots of hosts.<sup>[16]</sup> Therefore, the design of  $\text{Bi}^{3+}$ - $\text{Eu}^{3+}$  energy transfer is considered as a viable strategy to achieve tunable emission from blue/green to red, providing a possibility to realize white light-emitting in a single phase.

In this work,  $\text{Ca}_3\text{Ga}_4\text{O}_9$  (CGO) with a highly condensed framework and multiple Ca sites for  $\text{Bi}^{3+}$  doping was selected as the host to achieve the targeted cyan emission and  $\text{Bi}^{3+}$ - $\text{Eu}^{3+}$  energy transfer. Herein, the  $\text{CGO}:\text{Bi}^{3+}$  phosphor was prepared using the conventional high-temperature solid-state reaction, the cyan emission of which was enhanced significantly by incorporation of  $\text{Zn}^{2+}$ . Besides, the photoluminescence tuning of  $\text{CGO}:\text{Bi}^{3+}$  from cyan to yellowish-green and orange was achieved by codoping  $\text{La}^{3+}$  and  $\text{Bi}^{3+}$ - $\text{Eu}^{3+}$  energy

transfer, respectively. The photoluminescence properties were investigated in detail and the corresponding mechanisms are proposed. Temperature-dependent photoluminescence spectra indicate that the introduction of  $\text{Zn}^{2+}$  or  $\text{La}^{3+}$  improves the thermal stability of  $\text{CGO}:\text{Bi}^{3+}$ . Finally, a single-phased warm WLED was obtained by utilizing  $\text{CGO}:\text{Bi}^{3+}$ ,  $\text{Zn}^{2+}$ ,  $\text{Eu}^{3+}$  phosphor. Moreover, a full-spectrum WLED device by employing the developed cyan-emitting  $\text{CGO}:\text{Bi}^{3+},\text{Zn}^{2+}$  phosphor was generated with an excellent Ra of 97.4 and a high luminous efficiency of  $69.72$  lm  $\text{W}^{-1}$ , illustrating the vital role of  $\text{CGO}:\text{Bi}^{3+}$ ,  $\text{Zn}^{2+}$  phosphor in full-spectrum white lighting.

## 2. Results and Discussion

### 2.1. Phase Identification and Crystal Structure

The studied CGO has a condensed crystal structure framework constructed by the vertex-sharing gallium-oxygen  $\text{GaO}_4$  tetrahedrons, as presented in **Figure 1a**. Every four and five  $\text{GaO}_4$  tetrahedrons adjacent to each other form a  $\text{Ga}_4\text{O}_{12}$  four-membered tetrahedral ring and a  $\text{Ga}_5\text{O}_{15}$  five membered tetrahedral ring, respectively. Along the [001] direction, two types of ring channels are established by the stacking of  $\text{Ga}_4\text{O}_{12}$  rings and  $\text{Ga}_5\text{O}_{15}$  rings, respectively. In the CGO host lattice, there are four different Ca sites (named as Ca1, Ca2, Ca3 and Ca4). Ca1 and Ca3 are located in the four-membered ring channels while Ca2 and Ca4 are located in the five-membered ring channels. A two-dimensional gallium-oxygen planar structure on the *ab* plane is formed by  $\text{GaO}_4$  tetrahedrons, which is distributed alternately with the Ca atom layer in the [001] direction. The coordination polyhedrons of the four Ca sites are given in the bottom of **Figure 1a**. Ca1 and Ca3 are coordinated by six O atoms, while Ca2 and Ca4 are coordinated by eight O atoms.

**Figure 1b** shows the X-ray diffraction (XRD) patterns of the as-synthesized CGO host,  $\text{CGO}:0.02\text{Bi}^{3+}$ ,  $\text{CGO}:0.02\text{Bi}^{3+}, 0.07\text{Zn}^{2+}$  and  $\text{CGO}:0.02\text{Bi}^{3+}, 0.05\text{La}^{3+}$  phosphors. Almost all diffraction peaks of these samples can be well indexed with the standard data of CGO phase (PDF card No.83-1477), except for tiny peaks of  $\text{CaGa}_2\text{O}_4$  impurity (wt.  $\approx 2$ –4%) revealed by the Rietveld refinements, as displayed in **Figure 1c,d** and **Figure S1**, Supporting Information. The refinement results certify the successful formation of these CGO phase. Although the  $\text{CaGa}_2\text{O}_4\text{:Bi}^{3+}$  presents a yellow emission,<sup>[17]</sup> its influence on the luminescence of  $\text{CGO}:\text{Bi}^{3+}$  can be neglected due to the tiny amount. **Table 1** lists the main parameters of processing and refinement. It is confirmed that these as-studied phosphors crystallize in the orthorhombic phase with space group *Cmm2* (35). The cell parameters of the representative  $\text{CGO}:0.02\text{Bi}^{3+}$  sample are refined to be  $a = 14.3616(9)$  Å,  $b = 16.8136(11)$  Å,  $c = 5.3138(4)$  Å,  $V = 1283.13(14)$  Å<sup>3</sup>, and the reliability factors are  $R_{\text{wp}} = 5.10\%$ ,  $R_p = 3.91\%$ , and  $\chi^2 = 1.36$ . All the refinements show low *R*-factors and  $\chi^2$ , indicating the reliable refinement results and demonstrating that the doping of  $\text{Bi}^{3+}$ ,  $\text{Zn}^{2+}$  and  $\text{La}^{3+}$  ions do not influence the phase purity of the CGO host. Moreover, the fractional coordinates of atoms and main bond lengths are provided in **Table S1** and **S2**, Supporting Information, respectively.

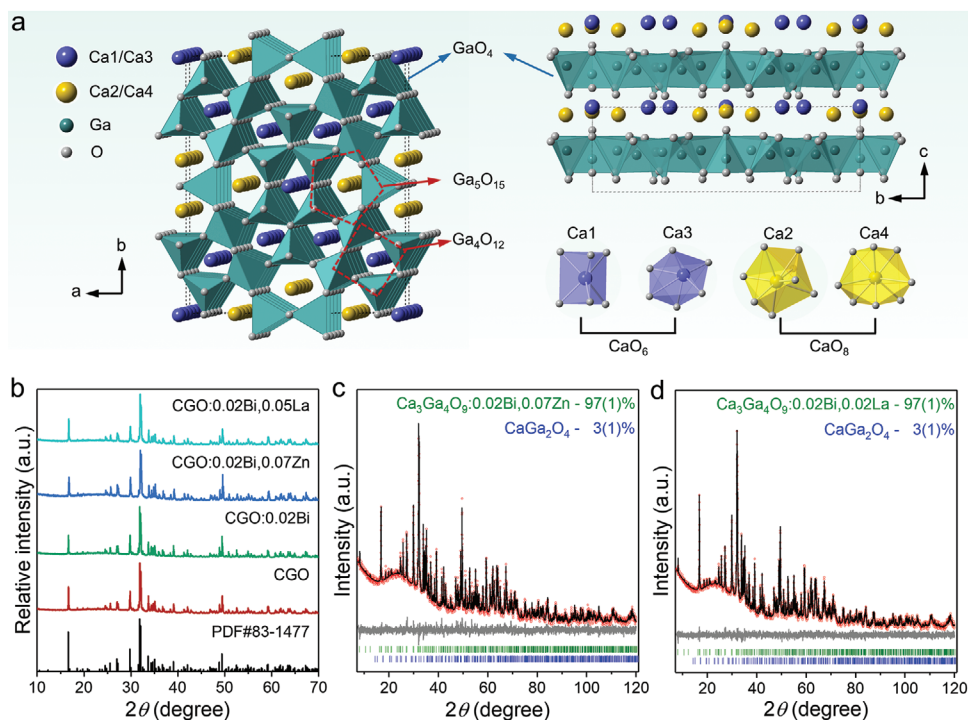


**Figure 1.** a) Schematic crystal structure of CGO host as well as coordination polyhedrons of Ca1–Ca4 with oxygen atoms. b) XRD patterns of CGO host, CGO:0.02Bi<sup>3+</sup>, CGO:0.02Bi<sup>3+</sup>, 0.07Zn<sup>2+</sup>, and CGO:0.02Bi<sup>3+</sup>, 0.05La<sup>3+</sup> phosphors. Rietveld refinements of the powder XRD patterns of c) CGO:0.02Bi<sup>3+</sup>, 0.07Zn<sup>2+</sup>, and d) CGO:0.02Bi<sup>3+</sup>, 0.02La<sup>3+</sup> phosphors.

The morphology and chemical compositions of the representative phosphors were further investigated using the scanning electron microscopy (SEM). **Figure 2a** reveals the irregular morphology of CGO:0.02Bi<sup>3+</sup> with particles agglomeration, the size of which is generally < 20 μm. Interestingly, with the introduction of Zn<sup>2+</sup>, the smaller particles of CGO:0.02Bi<sup>3+</sup> grow to a several times larger bulk crystal, as depicted in **Figure 2b**, which typically benefits its luminescence. The role of Zn<sup>2+</sup> in the system is somewhat similar to that of flux. Therefore, the stronger luminescence intensity of CGO:0.02Bi<sup>3+</sup>, 0.07Zn<sup>2+</sup> phosphor could be expected. As shown in **Figure 2c**, one CGO:0.02Bi<sup>3+</sup> particle is selected for the energy-dispersive X-ray spectroscopy (EDS) mapping images, confirming that the elements Ca, Ga, O and Bi

are homogeneously distributed in the region examined. In addition, the elemental mapping images of CGO:0.02Bi<sup>3+</sup>, 0.07Zn<sup>2+</sup>, and CGO:0.02Bi<sup>3+</sup>, 0.02La<sup>3+</sup> are given in **Figure S2**, Supporting Information, indicating the successful incorporation of Bi, Zn and La in corresponding phosphors.

## 2.2. Photoluminescence Properties

As the band gap of host matrix is essential to the luminescent property of a phosphor, density functional theory (DFT) calculations are used to study the electron properties of the CGO host.<sup>[18]</sup> **Figure 3a** presents the total density of states for CGO and the partial density of states for Ca, Ga and O atoms.

**Table 1.** Main parameters of processing and refinement of the representative samples.

Compound	CGO	CGO:0.02Bi <sup>3+</sup>	CGO:0.02Bi <sup>3+</sup> , 0.07Zn <sup>2+</sup>	CGO:0.02Bi <sup>3+</sup> , 0.02La <sup>3+</sup>
Space group	<i>Cmm2</i>	<i>Cmm2</i>	<i>Cmm2</i>	<i>Cmm2</i>
<i>a</i> , Å	14.3615 (12)	14.3616 (9)	14.3589 (19)	14.3631 (2)
<i>b</i> , Å	16.8126 (14)	16.8136 (11)	16.8134 (2)	16.8137 (2)
<i>c</i> , Å	5.3133 (5)	5.3138 (4)	5.3104 (8)	5.3138 (8)
<i>V</i> , Å <sup>3</sup>	1282.93 (18)	1283.13 (14)	1282.04 (3)	1283.26 (3)
<i>Z</i>	6	6	6	6
<i>R</i> <sub>w</sub> , %	5.10	5.10	6.24	5.29
<i>R</i> <sub>p</sub> , %	2.44	3.91	4.81	4.07
<i>R</i> <sub>B</sub> , %	1.36	2.44	3.02	1.51
χ <sup>2</sup>	1.36	1.36	1.32	1.15

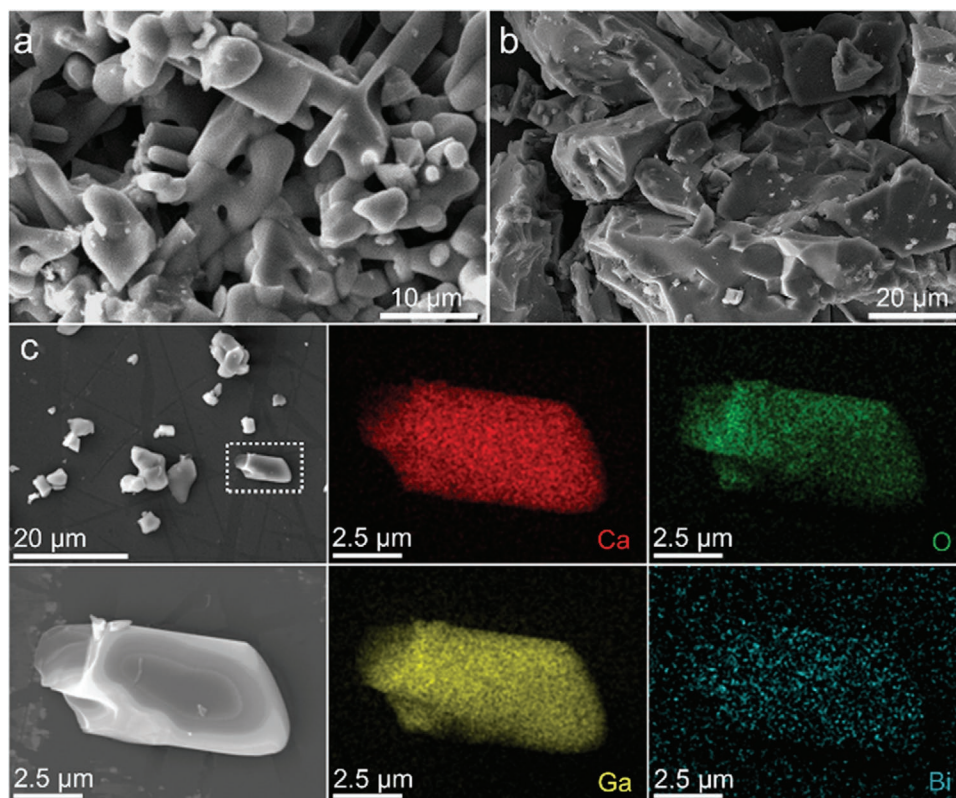


**Figure 2.** The SEM images of a) CGO:0.02Bi<sup>3+</sup> and b) CGO:0.02Bi<sup>3+</sup>, 0.07Zn<sup>2+</sup> phosphors. c) Element mapping images of Ca, Ga, O, and Bi elements in the selected CGO:0.02Bi<sup>3+</sup> phosphor particle.

According to the calculation results, the valence band (VB) is dominated by Ca 3p and O 2s2p states, while the conduction band (CB) is mainly composed of Ga 4s4p states. The band gap ( $E_g$ ) value of CGO was calculated to be 4.19 eV, which is close to the optical band gap (4.67 eV) obtained from the diffuse reflection (DR) spectrum according to the Kubelka-Munk absorption function:<sup>[10,19]</sup>

$$F(R) = (1 - R)^2 / 2R \quad (1)$$

$$[F(R) \times hv]^2 = A(hv - E_g) \quad (2)$$

where  $F(R)$  represents the absorption,  $R$  is the reflectance (%),  $hv$  is the photon energy, and  $E_g$  is the optical band gap, which can be estimated by extrapolating the linear portion of the  $[F(R) \times hv]^2$  versus  $hv$  curve, as shown in the inset of Figure 3b. The optical performances of the phosphors are investigated by the diffuse reflection spectra recorded in Figure 3b. The as-studied phosphors especially CGO:0.02Bi<sup>3+</sup>, 0.07Zn<sup>2+</sup> and CGO:0.02Bi<sup>3+</sup>, 0.05La<sup>3+</sup>, 0.04Zn<sup>2+</sup> have superior absorption in the range of 200–420 nm, matching well with the n-UV chips. These above results demonstrate that the CGO host is an available carrier for accommodating Bi<sup>3+</sup> as luminescence materials. Since the valence states of Bi can affect the luminescence properties, it is necessary to determine its valence in the CGO host.<sup>[20]</sup> Figure 3c plots the X-ray photoelectron spectroscopy (XPS) spectra of the representative phosphors. The typical Bi<sup>3+</sup> peaks at  $\approx 159$  and 164 eV can be

observed, which are assigned to Bi 4f<sub>7/2</sub> and Bi 4f<sub>5/2</sub>, respectively. This result suggests that the emission in CGO originates from trivalent Bi<sup>3+</sup> ions.

The photoluminescence spectra of CGO: $x$ Bi<sup>3+</sup> with different Bi<sup>3+</sup> doping concentration ( $0.01 \leq x \leq 0.05$ ) under 340 nm excitation are plotted in Figure S3, Supporting Information, which shows that the optimal doping concentration of Bi<sup>3+</sup> is  $x = 0.02$ . Figure 4a,b exhibit the excitation and emission spectra of CGO:0.02Bi<sup>3+</sup>,  $\gamma$ Zn<sup>2+</sup> ( $\gamma = 0-0.07$ ) phosphors, respectively. The excitation spectrum (monitored at  $\lambda_{em} = 490$  nm) of CGO:0.02Bi<sup>3+</sup> phosphor consists of a dominant peak at 340 nm and a shoulder peak at 290 nm, which are ascribed to the spin-allowed transition <sup>1</sup>S<sub>0</sub> → <sup>1</sup>P<sub>1</sub> ( $J = 3$  and 1) of Bi<sup>3+</sup>. Upon 370 nm excitation, the CGO:0.02Bi<sup>3+</sup> phosphor presents a broad emission band from 390 to 650 nm peaking at 486 nm. With the introduction of Zn<sup>2+</sup> ions, the excitation spectra of CGO:0.02Bi<sup>3+</sup>,  $\gamma$ Zn<sup>2+</sup> ( $\gamma = 0.01-0.07$ ) phosphors broaden to longer wavelength region. That is, the intensity of long wavelength excitation increases, implying that they have better absorption under n-UV chips. As for the emission spectra, there is nearly no change in peak shape and position. The full width at half-maximum (FWHM) of CGO:0.02Bi<sup>3+</sup>,  $\gamma$ Zn<sup>2+</sup> ( $\gamma = 0-0.07$ ) phosphors is  $\approx 96-99$  nm, which meets the requirement of broad cyan band proposed previously. Surprisingly, the emission intensity of Zn<sup>2+</sup> incorporated phosphors has remarkable enhancement compared to that of CGO:0.02Bi<sup>3+</sup> phosphor under both 370 and 340 nm excitation wavelengths (Figure 4b and Figure S4, Supporting Information). Figure 4c shows the

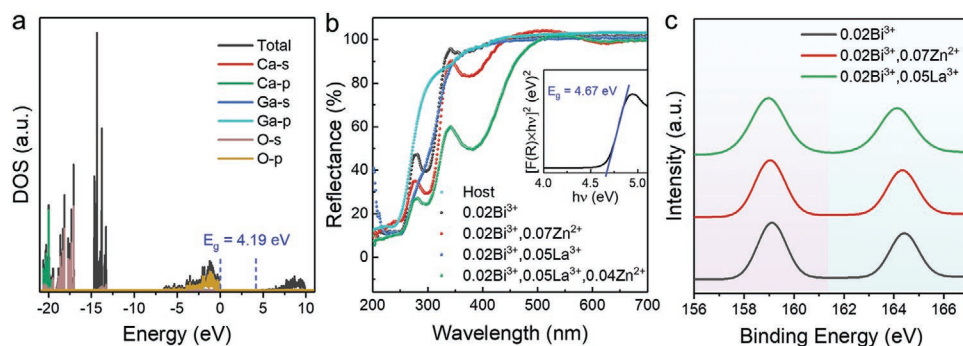


**Figure 3.** a) The projected electronic density of states (PDOS) of the CGO host obtained via DFT calculations. b) Diffuse reflectance spectra of CGO host, CGO:0.02Bi<sup>3+</sup>, CGO:0.02Bi<sup>3+</sup>, 0.07Zn<sup>2+</sup>, CGO:0.02Bi<sup>3+</sup>, 0.05La<sup>3+</sup>, and CGO:0.02Bi<sup>3+</sup>, 0.05La<sup>3+</sup>, 0.04Zn<sup>2+</sup> phosphors; the inset presents the calculated optical bandgap value of CGO host. c) XPS spectra of CGO:0.02Bi<sup>3+</sup>, CGO:0.02Bi<sup>3+</sup>, 0.07Zn<sup>2+</sup>, and CGO:0.02Bi<sup>3+</sup>, 0.05La<sup>3+</sup> phosphors.

integrated emission intensity of CGO:0.02Bi<sup>3+</sup>,  $\gamma$ Zn<sup>2+</sup> phosphor as a function of the doping concentration of Zn<sup>2+</sup> ions ( $\gamma$ ). Compared to Bi<sup>3+</sup> monodoped phosphor, the integrated emission intensity of CGO:0.02Bi<sup>3+</sup>, 0.07Zn<sup>2+</sup> phosphor increases by about 4.1 and 2.8 times excited at 370 and 340 nm, respectively. Even a little content of Zn doping still enhances the emission

intensity greatly ( $\approx 3.4$  times for  $\gamma = 0.01$  excited at 370 nm). The obvious increase in emission intensity for the studied cyan-emitting phosphor under 370 nm excitation is meaningful for the n-UV LED application. The inset in Figure 4c presents the corresponding luminescence photographs of CGO:0.02Bi<sup>3+</sup>,  $\gamma$ Zn<sup>2+</sup> phosphors under 365 nm UV lamp, which shows the

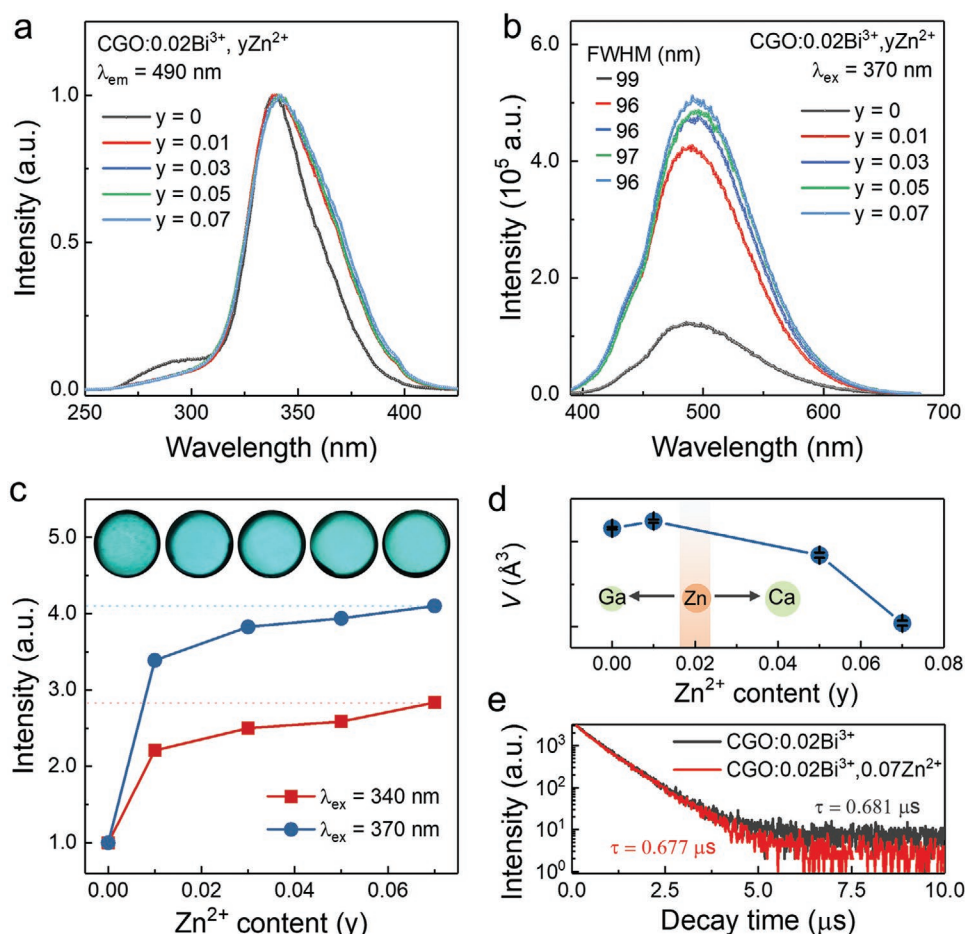


**Figure 4.** a) Photoluminescence excitation and b) photoluminescence spectra of CGO:0.02Bi<sup>3+</sup>,  $\gamma$ Zn<sup>2+</sup> ( $\gamma = 0$ –0.07) phosphors. c) The integrated emission intensity of CGO:0.02Bi<sup>3+</sup>,  $\gamma$ Zn<sup>2+</sup> ( $\gamma = 0$ –0.07) phosphors excited at 340 and 370 nm, respectively; the inset shows the corresponding luminescence photos of CGO:0.02Bi<sup>3+</sup>,  $\gamma$ Zn<sup>2+</sup> ( $\gamma = 0$ –0.07) phosphors under 365 nm excitation. d) Evolution of the unit cell volume  $V$  for CGO:0.02Bi<sup>3+</sup>,  $\gamma$ Zn<sup>2+</sup> ( $\gamma = 0$ –0.07) phosphors. e) Photoluminescence decay curves of CGO:0.02Bi<sup>3+</sup>,  $\gamma$ Zn<sup>2+</sup> ( $\gamma = 0$  and 0.07) phosphors under 375 nm excitation, monitored at 490 nm.

enhanced cyan emission intuitively. The internal quantum yields (IQYs) of CGO:0.02Bi<sup>3+</sup>,  $\gamma$ Zn<sup>2+</sup> ( $\gamma = 0-0.07$ ) phosphors are all above 50%, reaching the highest IQYs of 72.3% at  $\gamma = 0.01$  (Table S3, Supporting Information).

The effect of Zn<sup>2+</sup> on the emission of CGO:0.02Bi<sup>3+</sup> can be explained from two main aspects. On the one hand, the luminescence intensity is closely related to the morphology and size of phosphor particles. As discussed in the previous section, the large bulk crystal of Zn<sup>2+</sup> incorporated phosphor contributes to the improvement of the cyan emission. On the other hand, Bi<sup>3+</sup> ions tend to occupy Ca sites in CGO host owing to the similar ionic radii (Ca<sup>2+</sup>,  $r = 1.00$  Å, CN = 6;  $r = 1.12$  Å, CN = 8. Bi<sup>3+</sup>,  $r = 1.03$  Å, CN = 6;  $r = 1.17$  Å, CN = 8). However, a trivalent Bi<sup>3+</sup> substituting a divalent Ca<sup>2+</sup> leads to the charge imbalance and generates a cationic vacancy for the charge compensation in the Ca site. This vacancy can be reduced by another non-equivalent substitution, Zn<sup>2+</sup> substituting Ga<sup>3+</sup>. That is, the codoping of Bi<sup>3+</sup> and Zn<sup>2+</sup> into the CGO lattice generates the charge balance: Bi<sup>3+</sup> + Zn<sup>2+</sup> = Ca<sup>2+</sup> + Ga<sup>3+</sup>. Consequently, the emission intensity of CGO:0.02Bi<sup>3+</sup> increased obviously with the incorporation of Zn<sup>2+</sup> ( $\gamma \leq 0.02$ ). When  $\gamma > 0.02$ , Zn<sup>2+</sup> no longer acts as a charge compensator in CGO:0.02Bi<sup>3+</sup>,  $\gamma$ Zn<sup>2+</sup> because of the balanced charge. To further keep the charge balance, Zn<sup>2+</sup> is supposed mainly to occupy the Ca<sup>2+</sup> sites, which can be illustrated by the decreasing of cell volume with increasing  $\gamma$  values, as displayed in Figure 4d. The large difference of ionic radii between Zn<sup>2+</sup> ( $r = 0.74$  Å, CN = 6;  $r = 0.9$  Å, CN = 8) and Ca<sup>2+</sup> causes a crystal field distortion around Bi<sup>3+</sup>, resulting in the increased emission intensity. Figure 4e shows the room-temperature decay curves of CGO:0.02Bi<sup>3+</sup>,  $\gamma$ Zn<sup>2+</sup> ( $\gamma = 0$  and 0.07) phosphors monitored at 490 nm. The two decay curves were well fitted using a double exponential decay:<sup>[21]</sup>

$$I(t) = I_0 + A_1 \exp\left(\frac{-t}{\tau_1}\right) + A_2 \exp\left(\frac{-t}{\tau_2}\right) \quad (3)$$

The average luminescence lifetime  $\tau^*$  can be acquired from the following equation:

$$\tau^* = \frac{A_1\tau_1^2 + A_2\tau_2^2}{A_1\tau_1 + A_2\tau_2} \quad (4)$$

For  $\gamma = 0$  and  $\gamma = 0.07$  samples, the obtained average lifetimes are calculated to be 0.681 and 0.677  $\mu$ s, respectively. The close lifetime values indicate that Zn<sup>2+</sup> doping in CGO:0.02Bi<sup>3+</sup> has little influence on the luminescence decay of Bi<sup>3+</sup>.

Photoluminescence tuning is usually desired for phosphor materials to optimize and modify luminescence properties. As observed in Figure 5a, with the increase of excitation wavelengths from 280 to 400 nm, the normalized emission spectra of CGO:0.02Bi<sup>3+</sup> exhibit a large shift in the range of 478 to 532 nm, which indicates the existence of multiple luminescent centers in CGO:0.02Bi<sup>3+</sup>. Additionally, the normalized excitation spectra of CGO:0.02Bi<sup>3+</sup> monitored emission wavelengths from 420 to 650 nm are displayed in Figure 5b. The variation of the relative intensity of the two excitation peaks (centered at 290 and 340 nm) also reveals that there is more than one luminescent center in CGO:0.02Bi<sup>3+</sup>. To further confirm this, the emission spectrum of CGO:0.02Bi<sup>3+</sup> measured under 10 K is given

in Figure 5c. The emission band shows an asymmetric major peak and a small shoulder peak, which can be well deconvoluted into four peaks at 425, 500, 545, and 600 nm by Gaussian fitting, deriving from four luminescent centers in CGO:0.02Bi<sup>3+</sup>. These four Bi<sup>3+</sup> centers are attributed to Bi<sup>3+</sup> occupying four cation sites (Ca1–Ca4). To distinguish the site occupations of different Bi<sup>3+</sup> ions, crystal field splitting is introduced:<sup>[22]</sup>

$$D_q = \frac{1}{6} Z e^2 \frac{r^4}{R^5} \quad (5)$$

where  $D_q$  is the splitting energy,  $Z$  is the anion charge,  $e$  is the electron charge,  $r$  is the  $d$  wave function radius, and  $R$  is the bond length. The smaller  $R$  value results in the stronger of crystal field and subsequent longer-wavelength emission. According to the refinement results, the average bond lengths of Ca1–O, Ca2–O, Ca3–O, and Ca4–O in CGO are 2.365, 2.478, 2.419 and 2.587 Å, respectively. Therefore, Bi<sup>3+</sup>(1), Bi<sup>3+</sup>(2), Bi<sup>3+</sup>(3) and Bi<sup>3+</sup>(4) emission centers should be assigned to Ca1, Ca3, Ca2 and Ca4 sites, respectively.

The multiple cation sites provide a possibility of site-selected occupation of Bi<sup>3+</sup> ions and thus regulate the luminescence. Here, La<sup>3+</sup> ions were introduced in CGO:0.02Bi<sup>3+</sup> to realize luminescence tuning. CGO:0.02Bi<sup>3+</sup>,  $z$ La<sup>3+</sup> ( $z = 0-0.15$ ) were synthesized and the pure-phased phosphors were obtained at  $z \leq 0.05$  (Figure S5a, Supporting Information). Figure 5d shows the normalized emission spectra of CGO:0.02Bi<sup>3+</sup>,  $z$ La<sup>3+</sup> ( $z = 0-0.15$ ) phosphors under 370 nm excitation wavelength. A red shift from 486 to 528 nm can be achieved by incorporation of a few La<sup>3+</sup> ions in CGO:0.02Bi<sup>3+</sup>. Even at a really low doping content ( $z = 0.02$ ) of La<sup>3+</sup>, the similar red-shift emission can also be observed. The emission intensity of CGO:0.02Bi<sup>3+</sup>,  $z$ La<sup>3+</sup> ( $z = 0-0.15$ ) as a function of  $z$  is given in the inset of Figure 5d. The CIE chromaticity coordinates shift from (0.1960, 0.3481) to (0.2925, 0.5018) as  $z$  varies from 0 to 0.05 (Figure 5e). The excitation spectrum of CGO:0.02Bi<sup>3+</sup>, 0.05La<sup>3+</sup> is displayed in Figure S5b, Supporting Information, which shows a broad band from 250 to 425 nm centered at 340 nm. Figure S5c, Supporting Information, presents the emission spectrum of CGO:0.02Bi<sup>3+</sup>, 0.05La<sup>3+</sup> measured at 100 K, which is also deconvoluted into four peaks by Gaussian fitting, indicating the four different Bi<sup>3+</sup> emission centers. Figure 5f presents the Gaussian peaks of the room-temperature emission spectra of CGO:0.02Bi<sup>3+</sup>,  $z$ La<sup>3+</sup> ( $z = 0$  and 0.05). Clearly, Bi<sup>3+</sup> mainly occupies Ca2 and Ca3 sites in CGO:0.02Bi<sup>3+</sup>. However, the luminescence proportion of different Bi<sup>3+</sup> emission centers changes with the introduction of La<sup>3+</sup>. It is speculated that the codoping of La<sup>3+</sup> into CGO:0.02Bi<sup>3+</sup> causes the preferential occupation of Bi<sup>3+</sup> from Ca2 to Ca3 site. The photoluminescence decay curve of CGO:0.02Bi<sup>3+</sup>, 0.05La<sup>3+</sup> monitoring at 528 nm is collected in Figure S5d, Supporting Information. The prolonged lifetime (0.853  $\mu$ s) is consistent with red shift of the emission spectra, further confirming the spectral adjustment by site-selection of Bi<sup>3+</sup> ions. Under 340 nm excitation, the measured internal quantum efficiency of CGO:0.02Bi<sup>3+</sup>, 0.05La<sup>3+</sup> is about 32.6% (Table S3, Supporting Information).

For better application in pc-WLEDs, further emission tuning of CGO:0.02Bi<sup>3+</sup> phosphor is needed. Figure S6a, Supporting Information, shows the emission spectra of

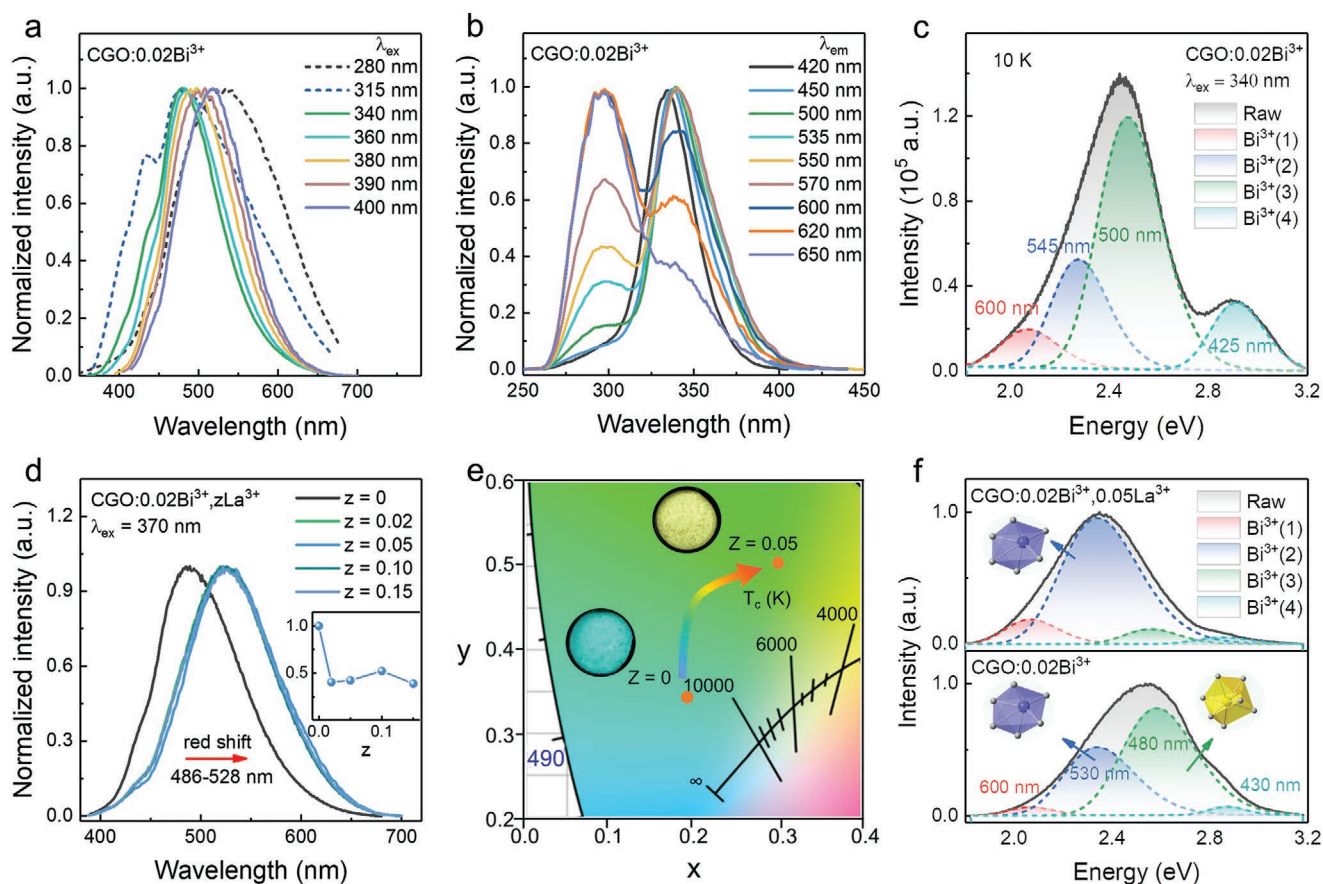


**Figure 5.** a) Normalized photoluminescence spectra of CGO:0.02Bi<sup>3+</sup> phosphor under different excitation wavelengths from 280 to 400 nm. b) Normalized photoluminescence excitation spectra of CGO:0.02Bi<sup>3+</sup> phosphor monitored at different emission wavelengths from 420 to 650 nm. c) The Gaussian fitting of the photoluminescence spectrum of CGO:0.02Bi<sup>3+</sup> phosphor excited with 340 nm wavelength at 10 K. d) Normalized photoluminescence spectra of CGO:0.02Bi<sup>3+</sup>, zLa<sup>3+</sup> (z = 0–0.15) phosphors upon 370 nm excitation; the inset shows the dependence of the relative emission intensity on La<sup>3+</sup> content (z) in CGO:0.02Bi<sup>3+</sup>, zLa<sup>3+</sup> phosphors. e) The CIE chromaticity coordinates under 370 nm excitation and luminescence photos under 365 nm of CGO:0.02Bi<sup>3+</sup>, zLa<sup>3+</sup> (z = 0 and 0.05) phosphors. f) The Gaussian fitting of the photoluminescence spectra of CGO:0.02Bi<sup>3+</sup>, zLa<sup>3+</sup> (z = 0 and 0.05) phosphors excited with 370 nm wavelength at room-temperature.

CGO:0.02Bi<sup>3+</sup>, 0.05La<sup>3+</sup>,  $\gamma$ Zn<sup>2+</sup> ( $\gamma = 0-0.04$ ) phosphors. It is noticed that the emission peaks undergo a gradual blue shift from 528 to 495 nm with the increase of Zn<sup>2+</sup> content. As discussed above, when Zn<sup>2+</sup> is incorporated in CGO:0.02Bi<sup>3+</sup>, the emission intensity is greatly enhanced but the peak shape and position have nearly no change. It is speculated that Zn<sup>2+</sup> could facilitate the luminescence of Bi<sup>3+</sup> in both Ca2 and Ca3 sites simultaneously. While La<sup>3+</sup> incorporation contributes to the preferential occupation of Bi<sup>3+</sup> in Ca3 site. Ca2 is the higher energy site whereas Ca3 is the lower energy site. Therefore, Zn<sup>2+</sup> codoping into CGO:0.02Bi<sup>3+</sup>, 0.05La<sup>3+</sup> can induce the blue-shift of emission. Meanwhile, the emission intensity enhances with the increase of Zn<sup>2+</sup> content (Figure S6b, Supporting Information). The corresponding CIE chromaticity coordinates and luminescence photographs of these samples are displayed in Figure S6c, Supporting Information.

Energy transfer is one of the common strategies to achieve spectral tuning and obtain single-phased white light emission. Herein, the CGO:0.02Bi<sup>3+</sup>, 0.07Zn<sup>2+</sup>, nEu<sup>3+</sup> (n = 0–0.15) phosphors were synthesized in pure phase (Figure S7a, Supporting Information). As shown in Figure S7b, Supporting Information,

there is obvious spectral overlap between the emission spectrum of CGO:0.02Bi<sup>3+</sup>, 0.07Zn<sup>2+</sup> and excitation spectrum of CGO:0.10Eu<sup>3+</sup>. Thus, the energy transfer from Bi<sup>3+</sup> to Eu<sup>3+</sup> is expected to occur in the CGO host. As presented in Figure 6a, the emission spectra of CGO:0.02Bi<sup>3+</sup>, 0.07Zn<sup>2+</sup>, nEu<sup>3+</sup> (n = 0–0.15) phosphors exhibit both the broad emission band of Bi<sup>3+</sup> and the sharp emission peaks of Eu<sup>3+</sup> (<sup>5</sup>D<sub>0</sub> → <sup>7</sup>F<sub>J</sub>, J = 0, 1, 2, 3, and 4).<sup>[13]</sup> As Eu<sup>3+</sup> concentration increases, the emission intensity of Bi<sup>3+</sup> monotonically decreases while that of Eu<sup>3+</sup> gradually increases, demonstrating the existence of energy transfer from Bi<sup>3+</sup> to Eu<sup>3+</sup> in CGO:0.02Bi<sup>3+</sup>, 0.07Zn<sup>2+</sup>, nEu<sup>3+</sup> (n = 0–0.15) phosphors. The luminescence photographs of these phosphors under 365 nm UV lamp excitation are given in Figure 6b, Supporting Information, which shows the emission tuning from cyan to orange across the white light region.

To further verify the existence of energy transfer from Bi<sup>3+</sup> to Eu<sup>3+</sup>, the photoluminescence decay curves of Bi<sup>3+</sup> in CGO:0.02Bi<sup>3+</sup>, 0.07Zn<sup>2+</sup>, nEu<sup>3+</sup> (n = 0–0.15) phosphors were measured and depicted in Figure 6c. These decay curves are also fitted with a double exponential decay. The calculated lifetimes of CGO:0.02Bi<sup>3+</sup>, 0.07Zn<sup>2+</sup>, nEu<sup>3+</sup> (n = 0–0.15) phosphors

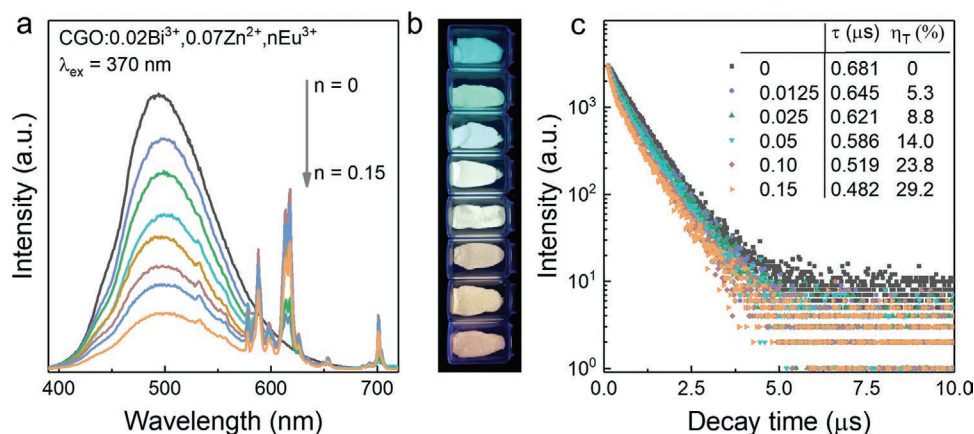


**Figure 6.** a) The photoluminescence spectra of CGO:0.02Bi<sup>3+</sup>, 0.07Zn<sup>2+</sup>, nEu<sup>3+</sup> (n = 0–0.15) phosphors under 370 nm excitation. b) Corresponding luminescence photos of CGO:0.02Bi<sup>3+</sup>, 0.07Zn<sup>2+</sup>, nEu<sup>3+</sup> (n = 0–0.15) phosphors under 365 nm UV lamp excitation. c) The photoluminescence decay curves of Bi<sup>3+</sup> emission in CGO:0.02Bi<sup>3+</sup>, 0.07Zn<sup>2+</sup>, nEu<sup>3+</sup> (n = 0–0.15) phosphors under 375 nm excitation, monitoring emission at 490 nm.

are listed in Figure 6c. With the increase of Eu<sup>3+</sup> concentration, the luminescent lifetimes of Bi<sup>3+</sup> gradually decrease from 0.681 to 0.482  $\mu$ s, which is consistent with the luminescent behavior of Bi<sup>3+</sup> in Figure 6a, strongly supporting the fact that the energy transfer from Bi<sup>3+</sup> to Eu<sup>3+</sup> exists. In addition, the energy transfer efficiency can be obtained using the following formula:<sup>[23]</sup>

$$\eta_T = 1 - \frac{\tau_n}{\tau_0} \quad (6)$$

where  $\tau_0$  and  $\tau_n$  are the corresponding lifetimes of Bi<sup>3+</sup> emission in the absence and presence of the acceptor Eu<sup>3+</sup>, respectively, and  $\eta_T$  is the calculated energy transfer efficiency. Accordingly, the efficiency of energy transfer from Bi<sup>3+</sup> to Eu<sup>3+</sup> gradually increases with the increase of Eu<sup>3+</sup> content, as displayed in Figure 6c. The maximum energy transfer efficiency reaches 29.2% for n = 15%. Therefore, the energy transfer from Bi<sup>3+</sup> to Eu<sup>3+</sup> is achieved for the controllable emission tuning and single-phased warm white light emitting. As discussed above, the schematic diagram for the optical tuning mechanism of CGO:0.02Bi<sup>3+</sup> is given vividly in Figure 7.

### 2.3. Thermal Stability and WLED Applications

The phosphors for WLEDs are required to have excellent thermal stability, since the working temperature of the high-power LED chips can reach up to 423 K.<sup>[5a,24]</sup> Figure 8a-d and Figure S8a, Supporting Information, show the temperature-dependent photoluminescence spectra of the as-studied phosphors, measured from 298 to 473 K under 370 nm excitation. All these phosphors have thermal quenching behaviors with increasing temperatures, but the emission quenching is slower with the Bi<sup>3+</sup>, Zn<sup>2+</sup> codoped phosphor. The normalized integrated emission intensities of these phosphors under different temperatures are displayed in Figure 8e. The Bi<sup>3+</sup>, Zn<sup>2+</sup> codoped phosphor shows the highest resistance to thermal quenching with about 76% emission intensity remaining at 423 K, which shows an improvement compared to that of Bi<sup>3+</sup> singly doped phosphor (68%). After codoping with La<sup>3+</sup>, the

CGO:0.02Bi<sup>3+</sup> phosphor presents better thermal stability at elevated temperatures (> 398 K, 71% remaining at 423 K). The improved thermal stability could be ascribed to the local lattice modification of CGO host by Zn<sup>2+</sup> and La<sup>3+</sup>. It is noticed that the thermal stability of the Bi<sup>3+</sup>, Zn<sup>2+</sup>, and La<sup>3+</sup> codoped phosphor declines a little with comparison to that of CGO:0.02Bi<sup>3+</sup> phosphor. It might be contributed to the negative effect of Zn<sup>2+</sup> and La<sup>3+</sup> codoping on the host lattice. Although the thermal

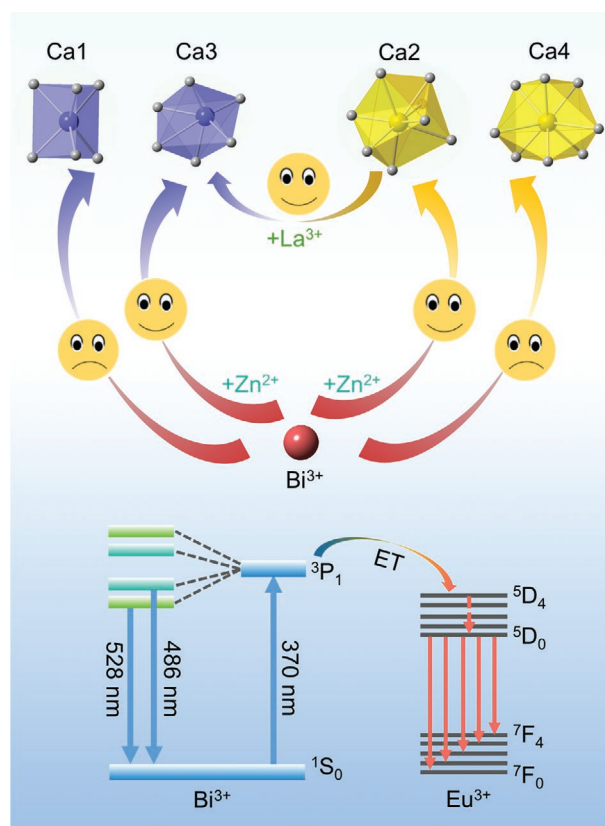


**Figure 7.** Schematic diagram for the optical tuning mechanism of CGO:0.02Bi<sup>3+</sup>.



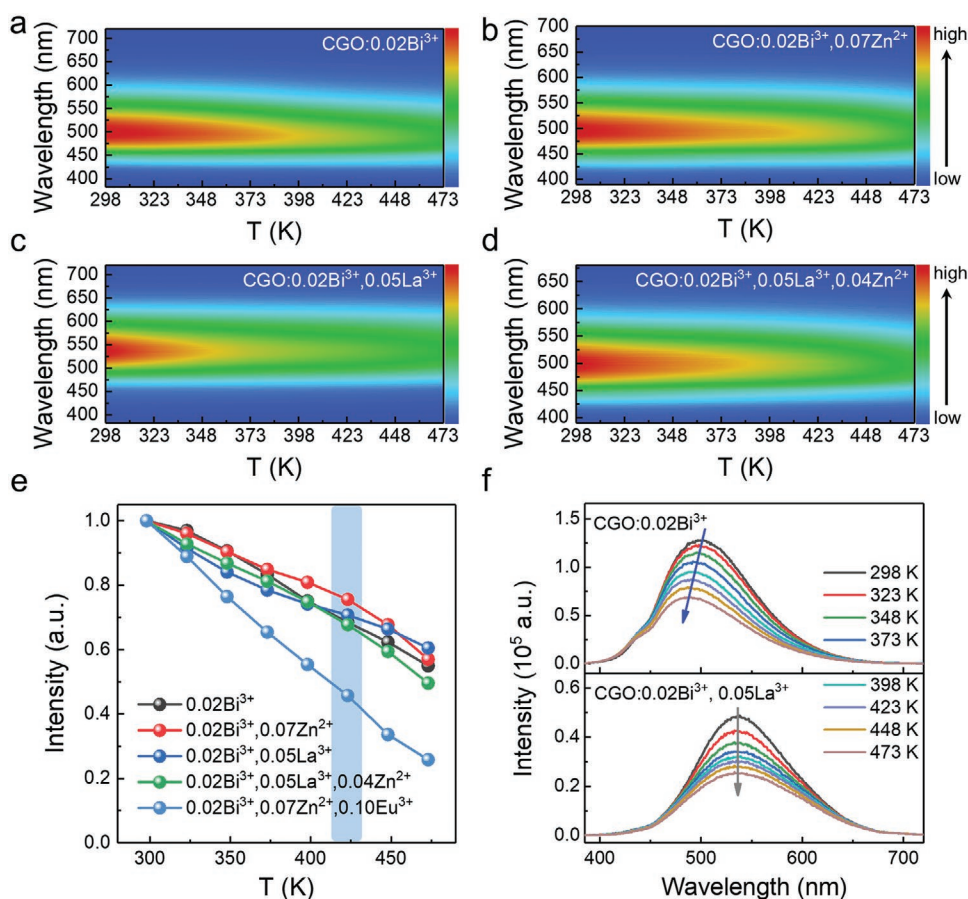


**Figure 8.** Temperature-dependent photoluminescence spectral profiles from 298 to 473 K for a) CGO:0.02Bi<sup>3+</sup>, b) CGO:0.02Bi<sup>3+</sup>, 0.07Zn<sup>2+</sup>, c) CGO:0.02Bi<sup>3+</sup>, 0.05La<sup>3+</sup>, and d) CGO:0.02Bi<sup>3+</sup>, 0.05La<sup>3+</sup>, 0.04Zn<sup>2+</sup> phosphors. e) Normalized emission intensity as a function of temperature of the phosphors. f) The compared temperature-dependent photoluminescence spectra of CGO:0.02Bi<sup>3+</sup> and CGO:0.02Bi<sup>3+</sup>, 0.05La<sup>3+</sup> phosphors.

stability of CGO:0.02Bi<sup>3+</sup>, 0.07Zn<sup>2+</sup>, 0.10Eu<sup>3+</sup> phosphor is not so good, it has a good color thermal stability as the emission intensity of Bi<sup>3+</sup> and Eu<sup>3+</sup> almost decreases synchronously with increasing temperature (Figure S8b, Supporting Information). As displayed in Figure 8f, there is an obvious blue shift in emission spectra of CGO:0.02Bi<sup>3+</sup> phosphor, which probably comes from thermally active phonon-assisted tunneling process<sup>[14]</sup> as well as the existence of multiple Bi<sup>3+</sup> emission centers with different thermal quenching behaviors. Moreover, the crystal field decreases due to the lattice expansion at high temperatures, resulting in the blue shift of emission spectra. However, the CGO:0.02Bi<sup>3+</sup>, 0.05La<sup>3+</sup> phosphor shows nearly no emission shift with increasing temperature, which could be attributed to the lattice modification effect of La<sup>3+</sup> on the host.

To evaluate the potential prospect of the CGO:0.02Bi<sup>3+</sup>, 0.07Zn<sup>2+</sup> cyan-emitting phosphor in high-quality full-spectrum white lighting applications, several prototype pc-LED devices were fabricated with different compositions using 370 nm UV chips. **Figure 9** shows the electroluminescence (EL) spectra of the as-fabricated LED devices under a driven current of 100 mA. The corresponding luminescence photographs of these LEDs are also presented. It can be seen that the LED-a fabricated by CGO:0.02Bi<sup>3+</sup>, 0.07Zn<sup>2+</sup> phosphor shows bright cyan emission with broad emission band effectively covering the spectral region

from 480 to 520 nm, which indicates that it can be employed in compensating the cyan gap. LED-b fabricated by a single-phased CGO:0.02Bi<sup>3+</sup>, 0.07Zn<sup>2+</sup>, 0.10Eu<sup>3+</sup> phosphor glows bright warm white light with Ra = 88.0, CCT = 3800 K and chromaticity coordinates of (0.40, 0.42), indicating the achievement of single-phased warm white emission. LED-c containing CGO:0.02Bi<sup>3+</sup>, 0.07Zn<sup>2+</sup> and commercial CaAlSiN<sub>3</sub>:Eu<sup>2+</sup> phosphors exhibits a continuous broadband emission spectrum, covering the whole visible region without the cyan cavity. The warm white light shows high Ra = 93.3, low CCT = 4218 K and CIE coordinates of (0.37, 0.39). Furthermore, for further evaluating the ability of CGO:0.02Bi<sup>3+</sup>, 0.07Zn<sup>2+</sup> cyan phosphor in closing the cyan gap, LED-d was fabricated by the combination of commercial RGB (namely, BAM:Eu<sup>2+</sup>, β-SiAlON:Eu<sup>2+</sup> and CaAlSiN<sub>3</sub>:Eu<sup>2+</sup>) phosphors. There is a significant cyan gap, which limits the improvement of Ra. As a result, LED-d gives a Ra lower than 90. The LED-e was obtained by addition of extra CGO:0.02Bi<sup>3+</sup>, 0.07Zn<sup>2+</sup> cyan phosphor into the above LED-d. Impressively, the LED-e shows high-quality white emission with Ra = 97.4, CCT = 5125 K and CIE coordinates of (0.34, 0.35). In comparison with LED-d, the Ra value of LED-e is improved significantly due to the compensation of the cyan gap. Besides, R9 and R12 are also important parameters of the WLED devices, which represent the red and blue light saturation of WLEDs, respectively. As summarized

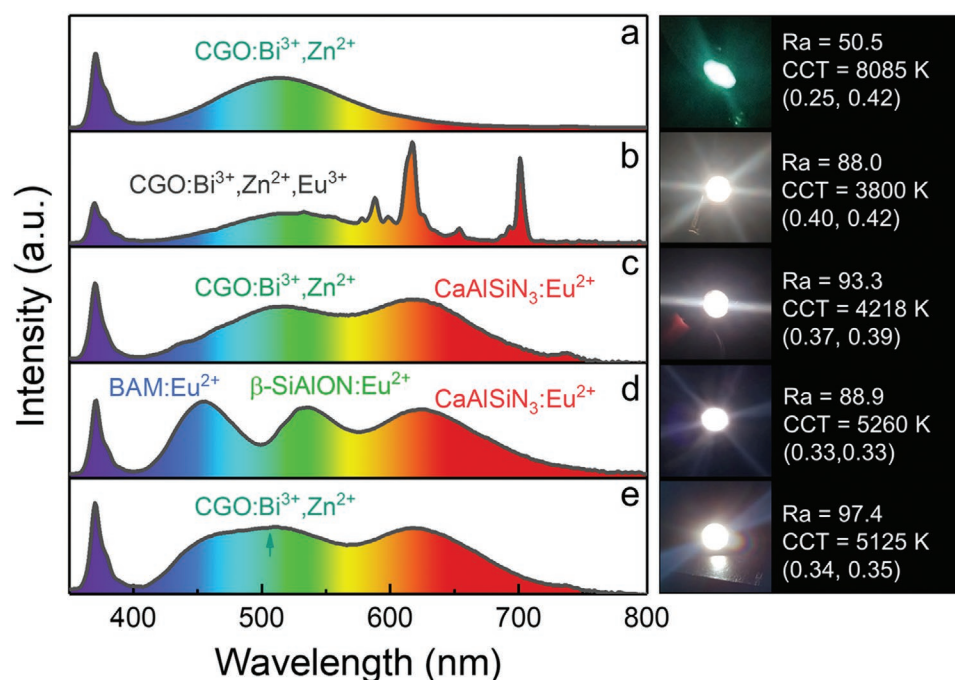


**Figure 9.** EL spectra and digital luminescence photographs of cyan and white LEDs fabricated by 370 nm UV chips coated with a) CGO:0.02Bi<sup>3+</sup>, 0.07Zn<sup>2+</sup> phosphor, b) CGO:0.02Bi<sup>3+</sup>, 0.07Zn<sup>2+</sup>, 0.10Eu<sup>3+</sup> phosphor, c) CGO:0.02Bi<sup>3+</sup>, 0.07Zn<sup>2+</sup> and commercial CaAlSiN<sub>3</sub>:Eu<sup>2+</sup> phosphors, d) commercial RGB (CaAlSiN<sub>3</sub>:Eu<sup>2+</sup>, β-SiAlON:Eu<sup>2+</sup>, BAM:Eu<sup>2+</sup>) phosphors, and e) CGO:0.02Bi<sup>3+</sup>, 0.07Zn<sup>2+</sup>, and commercial RGB phosphors, respectively.

in Tables S5, Supporting Information, both LED-c and LED-e possess high R9 and R12 values, indicating good color rendition ability. In addition, the luminous efficiencies of the two LEDs are measured to be 54.5 and 69.7 lm W<sup>-1</sup>, respectively (Table S5, Supporting Information). Since the difference between LED-c and LED-e is whether use commercial blue and green phosphors, the improved luminous efficiency of LED-e may be attributed to the excellent luminescence property of the commercial phosphors. Besides, the luminous efficiency is also related to the process treatment, which can be further optimized. The above results demonstrate that the as-prepared CGO:0.02Bi<sup>3+</sup>, 0.07Zn<sup>2+</sup> cyan phosphor is suitable for covering the cyan cavity and is promising in full-spectrum WLEDs for enhanced color rendition.

### 3. Conclusions

In this work, a series of Bi<sup>3+</sup>, Zn<sup>2+</sup>, La<sup>3+</sup>, Eu<sup>3+</sup> doped CGO phosphors were prepared via a high-temperature solid-state reaction. The XRD patterns and Rietveld refinement results reveal that these as-prepared samples crystallized in an orthorhombic phase with space group *Cmm2* (35). The CGO host has four Ca sites (Ca1–Ca4), and Bi<sup>3+</sup> ions are suggested to preferentially occupy the Ca2 and Ca3 sites in CGO:0.02Bi<sup>3+</sup> phosphor, showing a cyan emission at 486 nm under 370 nm excitation. By incorporating Zn<sup>2+</sup>, the intensity of the cyan emission can be increased by about 4.1 times due to the effect of morphology and size of phosphor particles, charge compensation, and lattice distortion. In addition, the emission red-shift from 486 to 528 nm is observed by doping La<sup>3+</sup> into CGO:0.02Bi<sup>3+</sup> phosphor, which is ascribed to the site preference of Bi<sup>3+</sup> luminescence

centers from Ca2 and Ca3 sites to mainly Ca3 site. Besides, the emission blue-shift from 528 to 495 nm is realized by codoping Zn<sup>2+</sup> into CGO:0.02Bi<sup>3+</sup>, 0.05La<sup>3+</sup> phosphor. Further, the photoluminescence tuning from cyan to orange could be achieved by the energy transfer from Bi<sup>3+</sup> to Eu<sup>3+</sup> in the as-prepared CGO:0.02Bi<sup>3+</sup>, 0.07Zn<sup>2+</sup>, nEu<sup>3+</sup> phosphors. The improved thermal stability was observed in Zn and La doped phosphors, and at 423 K the emission intensity can remain 76% and 71% of the initial room-temperature intensity, respectively. Finally, a warm WLED device with Ra = 88 and CCT = 3800 K was obtained by coating the single-phased CGO:0.02Bi<sup>3+</sup>, 0.07Zn<sup>2+</sup>, 0.10Eu<sup>3+</sup> phosphor on a 370 nm n-UV chip. Moreover, by utilizing the developed CGO:0.02Bi<sup>3+</sup>, 0.07Zn<sup>2+</sup> cyan phosphor, a full-spectrum WLED device was obtained with excellent performances including a remarkable Ra of 97.4 and a high luminous efficiency of 69.72 lm W<sup>-1</sup>, indicating that this phosphor is quite promising for realization of full-spectrum white lighting.

### 4. Experimental Section

**Materials and Preparation:** A series of Bi<sup>3+</sup>, Zn<sup>2+</sup>, La<sup>3+</sup>, Eu<sup>3+</sup> doped CGO phosphors were prepared by a traditional high temperature solid-state reaction using CaCO<sub>3</sub> (Aladdin, A. R.), Ga<sub>2</sub>O<sub>3</sub> (Aladdin, 99.99%), ZnO (Aladdin, 99.99%), La<sub>2</sub>O<sub>3</sub> (Aladdin, 99.99%), Bi<sub>2</sub>O<sub>3</sub> (Aladdin, A. R.), and Eu<sub>2</sub>O<sub>3</sub> (Aladdin, 99.99%) as the starting materials. The starting materials were weighed and mixed in an agate mortar by thoroughly grinding. After, the mixtures were put in alumina crucibles, which were then heated to 1483 K in a box furnace with a heating rate of 5 K min<sup>-1</sup> and held at this temperature for 10 h. The resulting products were slowly cooled and crushed finely to powder for further characterization.

**LED Fabrication:** Five LED devices were fabricated by the following combinations: 1) 370 nm chip + CGO:0.02Bi<sup>3+</sup>, 0.07Zn<sup>2+</sup> phosphor, 2) 370 nm chip + CGO:0.02Bi<sup>3+</sup>, 0.07Zn<sup>2+</sup>, 0.10Eu<sup>3+</sup> phosphor, 3) 370 nm chip + CGO:0.02Bi<sup>3+</sup>, 0.07Zn<sup>2+</sup> and commercial CaAlSiN<sub>3</sub>:Eu<sup>2+</sup> phosphors, 4) 370 nm chip + commercial RGB (CaAlSiN<sub>3</sub>:Eu<sup>2+</sup>, β-SiAlON:Eu<sup>2+</sup>, BAM:Eu<sup>2+</sup>) phosphors, 5) 370 nm chip + CGO:0.02Bi<sup>3+</sup>, 0.07Zn<sup>2+</sup>, and commercial RGB phosphors. Phosphors were first mixed thoroughly with epoxy resins and then coated on the 370 nm chips. The mixtures were cured at 150°C for 1 hour to form the final WLED devices for the electroluminescence performance measurements.

**Characterization:** The crystal phases of the as-prepared samples were identified by the XRD measurements on a Bruker D8 diffractometer operating with Cu Kα radiation (λ = 1.54 Å) at 40 kV and 40 mA. The scanning speed is 1° min<sup>-1</sup> and the 2θ range is 5–120°. XRD Rietveld refinements were performed with the TOPAS 4.2 to reveal the crystal structure and phase purity. The morphology and elemental composition of the samples were obtained by the field-emission SEM (S-4800, Hitachi) with an EDS spectrometer equipped. A Hitachi U-4100 UV–vis–NIR spectrophotometer using the white BaSO<sub>4</sub> for calibration recorded the DR spectra of the samples. Thermo SCIENTIFIC ESCALAB 250Xi with an Al Kα source was used to measure the XPS spectra. The room-temperature excitation and emission spectra were measured on an Edinburgh Instruments FLSP-920 fluorescence spectrometer attached with a 450 W xenon lamp. The photoluminescence lifetime decay curves were also recorded by the same spectrometer equipped with 375 nm laser. The absolute photoluminescence quantum efficiency measurement system (C9920–02, Hamamatsu photonics K. K., Japan) was applied to measure the photoluminescence quantum yields. The thermal stabilities were determined by the FLSP-920 spectrometer connected with a temperature controller. The EL performances of the as-fabricated WLEDs were evaluated by using a 150 integral sphere on Starspec SSP6612 apparatus.

**Computation:** The first-principle DFT calculations were carried out to investigate the density of states of CGO host using the Vienna ab initio simulation package (VASP) code.<sup>[25]</sup> Ca 3p<sup>6</sup>4s<sup>2</sup>, Ga 4s<sup>2</sup>4p<sup>1</sup> and O 2s<sup>2</sup>2p<sup>4</sup> electrons were used as the valence electrons and the electron-ion interaction was treated with the projector augmented wave (PAW) method.<sup>[26]</sup> The hybrid functional Heyd–Scuseria–Ernzerh (HSE) was chosen to describe the exchange and correlation functional. The structure relaxations were performed with a 400 eV plane-wave cutoff. The self-consistent total-energy difference and the convergence criterion for the forces on the atoms were set to 10<sup>-3</sup> eV and -0.01 eV Å<sup>-1</sup>, respectively. 2 × 2 × 5 Monkhorst-Pack grid for CGO was selected for k-point integration within the first Brillouin zone.

## Supporting Information

Supporting Information is available from the Wiley Online Library or from the author.

## Acknowledgements

This work was financially supported by the National Natural Science Foundation of China (NSFC No. 51932009, 51720105015, 51672265, 51672266, 51672257 and 51672259), the Key Research Program of Frontier Sciences, CAS (Grant No. YZDY-SSW-JSC018), Science and Technology Cooperation Project between Chinese and Australian Governments (2017YFE0132300), the Jiangmen Innovative Research Team Program (2017), and the Major Program of Basic Research and Applied Research of Guangdong Province (2017KZDXM083).

## Conflict of Interest

The authors declare no conflict of interest.

## Keywords

cyan-emitting phosphors, full-spectrum white lighting, optical tuning, single-phased white light-emitting diodes

Received: June 23, 2020

Revised: August 14, 2020

Published online: September 21, 2020

- a) G. Li, Y. Tian, Y. Zhao, J. Lin, *Chem. Soc. Rev.* **2015**, *44*, 8688; b) E. F. Schubert, J. K. Kim, *Science* **2005**, *308*, 1274; c) M. Zhao, H. Liao, M. S. Molokeev, Y. Zhou, Q. Zhang, Q. Liu, Z. Xia, *Light: Sci. Appl.* **2019**, *8*, 38; d) S. Ye, F. Xiao, Y. X. Pan, Y. Y. Ma, Q. Y. Zhang, *Mater. Sci. Eng., R* **2010**, *71*, 1.
- a) H. Zhu, C. C. Lin, W. Luo, S. Shu, Z. Liu, Y. Liu, J. Kong, E. Ma, Y. Cao, R.-S. Liu, X. Chen, *Nat. Commun.* **2014**, *5*, 4312; b) S. Nakamura, *MRS Bull.* **1997**, *22*, 29; c) L. Wang, R.-J. Xie, T. Suehiro, T. Takeda, N. Hirosaki, *Chem. Rev.* **2018**, *118*, 1951.
- a) N. C. George, K. A. Denault, R. Seshadri, *Annu. Rev. Mater. Sci.* **2013**, *43*, 481; b) J. Meyer, F. Tappe, *Adv. Opt. Mater.* **2015**, *3*, 424; c) Y. Wei, G. Xing, K. Liu, G. Li, P. Dang, S. Liang, M. Liu, Z. Cheng, D. Jin, J. Lin, *Light: Sci. Appl.* **2019**, *8*, 15.
- a) J. H. Oh, S. J. Yang, Y. R. Do, *Light: Sci. Appl.* **2014**, *3*, e141; b) T. Ueda, T. Nakanishi-Ueda, H. Yasuhara, R. Koide, W. W. Dawson, *Exp. Eye Res.* **2009**, *89*, 863; c) C. Moderie, S. Van der Maren, M. Dumont, *Sleep Med* **2017**, *34*, 148; d) L. Bellia, F. Bisegna, G. Spada, *Build. Environ.* **2011**, *46*, 1984.
- a) J. Qiao, L. Ning, M. S. Molokeev, Y.-C. Chuang, Q. Liu, Z. Xia, *J. Am. Chem. Soc.* **2018**, *140*, 9730; b) Y. Wei, L. Cao, L. Lv, G. Li, J. Hao, J. Gao, C. Su, C. C. Lin, H. S. Jang, P. Dang, J. Lin, *Chem. Mater.* **2018**, *30*, 2389; c) K. Uheda, N. Hirosaki, Y. Yamamoto, A. Naito, T. Nakajima, H. Yamamoto, *Electrochem. Solid-State Lett.* **2006**, *9*, H22; d) R. J. Xie, N. Hirosaki, H. L. Li, Y. Q. Li, M. Mitomo, *J. Electrochem. Soc.* **2007**, *154*, J314.
- a) J. Zhong, Y. Zhuo, S. Hariyani, W. Zhao, J. Wen, J. Brgoch, *Chem. Mater.* **2020**, *32*, 882; b) P. Dang, D. Liu, Y. Wei, G. Li, H. Lian, M. Shang, J. Lin, *Inorg. Chem.* **2020**, *59*, 6026; c) J. Liang, B. Devakumar, L. Sun, S. Wang, Q. Sun, X. Huang, *J. Mater. Chem. C* **2020**, *8*, 4934.
- P. Strobel, T. de Boer, V. Weiler, P. J. Schmidt, A. Moewes, W. Schnick, *Chem. Mater.* **2018**, *30*, 3122.
- S. Ray, P. Tadge, S. J. Dhoble, G. B. Nair, A. Singh, A. K. Singh, M. Rai, T. M. Chen, V. Rajput, *J. Alloys Compd.* **2017**, *713*, 138.
- Y. Zheng, W. Zhuang, X. Xing, J. Zhong, R. Liu, Y. Li, Y. Liu, Y. Hu, *RSC Adv.* **2016**, *6*, 68852.
- J. Han, F. Pan, M. S. Molokeev, J. Dai, M. Peng, W. Zhou, J. Wang, *ACS Appl. Mater. Interfaces* **2018**, *10*, 13660.
- a) J. Han, L. Li, M. Peng, B. Huang, F. Pan, F. Kang, L. Li, J. Wang, B. Lei, *Chem. Mater.* **2017**, *29*, 8412; b) F. Kang, H. Zhang, L. Wondraczek, X. Yang, Y. Zhang, D. Y. Lei, M. Peng, *Chem. Mater.* **2016**, *28*, 7807.
- L. Wang, J. Qiao, Y. Liu, P. Huang, Q. Shi, Y. Tian, C. Cui, Z. Luo, *Opt. Mater.* **2017**, *67*, 78.
- D. Liu, P. Dang, X. Yun, G. Li, H. Lian, J. Lin, *J. Mater. Chem. C* **2019**, *7*, 13536.
- P. Dang, S. Liang, G. Li, H. Lian, M. Shang, J. Lin, *J. Mater. Chem. C* **2018**, *6*, 9990.
- a) X. Y. Liu, H. Guo, Y. Liu, S. Ye, M. Y. Peng, Q. Y. Zhang, *J. Mater. Chem. C* **2016**, *4*, 2506; b) A. Huang, Z. Yang, C. Yu, Z. Chai, J. Qiu, Z. Song, *J. Phys. Chem. C* **2017**, *121*, 5267; c) F. Kang, Y. Zhang, M. Peng, *Inorg. Chem.* **2015**, *54*, 1462.
- a) R. Wangkhem, T. Yaba, N. S. Singh, R. S. Ningthoujam, *J. Appl. Phys.* **2018**, *123*, 124303; b) W. Wang, Z. Sun, X. He, Y. Wei, Z. Zou, J. Zhang, Z. Wang, Z. Zhang, Y. Wang, *J. Mater. Chem. C* **2017**,

- 5, 4310; c) W. Chen, Z. Liu, L. Shen, C. Shen, L. Ding, Z. Zhang, H. Zhang, W. Xiang, X. Liang, *J. Mater. Sci.* **2019**, *54*, 4056; d) Y. Ma, W. Ran, W. Li, C. Ren, H. Jiang, J. Shi, *Luminescence* **2016**, *31*, 665.
- [17] S. Wang, W. Chen, D. Zhou, J. Qiu, X. Xu, X. Yu, *J. Am. Ceram. Soc.* **2017**, *100*, 3514.
- [18] a) J. Zhong, W. Zhao, F. Du, J. Wen, W. Zhuang, R. Liu, C.-K. Duan, L. Wang, K. Lin, *J. Phys. Chem. C* **2018**, *122*, 7849; b) X. Qin, X. Liu, W. Huang, M. Bettinelli, X. Liu, *Chem. Rev.* **2017**, *117*, 4488.
- [19] L. Liu, Y. Yang, Q. Jing, X. Dong, Z. Yang, S. Pan, K. Wu, *J. Phys. Chem. C* **2016**, *120*, 18763.
- [20] a) F. Kang, M. Peng, *Dalton Trans.* **2014**, *43*, 277; b) G. Zhou, X. Jiang, J. Zhao, M. Molokeev, Z. Lin, Q. Liu, Z. Xia, *ACS Appl. Mater. Interfaces* **2018**, *10*, 24648.
- [21] a) D. L. Dexter, J. H. Schulman, *J. Chem. Phys.* **1954**, *22*, 1063; b) S. Wang, S. Ma, G. Zhang, Z. Ye, X. Cheng, *ACS Appl. Mater. Interfaces* **2019**, *11*, 42330; c) Z. Xia, C. Ma, M. S. Molokeev, Q. Liu, K. Rickert, K. R. Poeppelmeier, *J. Am. Chem. Soc.* **2015**, *137*, 12494.
- [22] a) M. Shang, C. Li, J. Lin, *Chem. Soc. Rev.* **2014**, *43*, 1372; b) M. Zhang, Z. Xia, M. S. Molokeev, L. Shi, Q. Liu, *J. Mater. Chem. C* **2016**, *4*, 9078; c) G. Blasse, *Prog. Solid State Chem.* **1988**, *18*, 79.
- [23] a) W. Lu, H. Xu, J. Huo, B. Shao, Y. Feng, S. Zhao, H. You, *Dalton Trans.* **2017**, *46*, 9272; b) Y. Tian, Y. Wei, Y. Zhao, Z. Quan, G. Li, J. Lin, *J. Mater. Chem. C* **2016**, *4*, 1281.
- [24] Y. H. Kim, P. Arunkumar, B. Y. Kim, S. Unithrattil, E. Kim, S.-H. Moon, J. Y. Hyun, K. H. Kim, D. Lee, J.-S. Lee, W. B. Im, *Nat. Mater.* **2017**, *16*, 543.
- [25] a) J. Hafner, *J. Comput. Chem.* **2008**, *29*, 2044; b) S. L. Dudarev, G. A. Botton, S. Y. Savrasov, C. J. Humphreys, A. P. Sutton, *Phys. Rev. B* **1998**, *57*, 1505.
- [26] P. E. Blochl, *Phys. Rev. B* **1994**, *50*, 17953.